JOURNAL OF SOLID STATE CHEMISTRY 50, 7–19 (1983)

Electron Microscope Studies of Sodium and Lithium Intercalation in TiS_2

D. CHERNS* AND G. P. NGO

Department of Metallurgy and Science of Materials, University of Oxford, Parks Road, Oxford OX1 3PH, England

Received March 28, 1983; in revised form June 15, 1983

Lithium and sodium intercalation in TiS_2 have been studied by transmission electron microscopy using lattice imaging and diffraction contrast techniques. Na_xTiS_2 samples ($0 \leq x \leq 0.6$) from Na/NaI in propylene carbonate/TiS_2 batteries were found to contain a complex variety of phases inhomogeneous on a fine scale. Observations showed variable staging and a 2H phase not previously reported for this system at ambient temperatures. Observations on both Na_xTiS_2 and chemically prepared Li_xTiS_2 showed highly dislocated structures. A model is proposed whereby dislocations are introduced to accommodate misfit strains caused by nonuniform intercalation and, in the case of Na_xTiS_2, to initiate phase transformations, leading to potentially irreversible structural changes in cycled material.

Introduction

The ability of layered transition metal dichalogenides to act as hosts for the intercalation of alkali ions and also as good ionic and electronic conductors has led to their investigation as possible electrode materials for advanced battery systems. The chemistry of intercalation and the broad phase changes which occur over battery charge/discharge cycles have been widely studied (e.g., for a review see Whittingham (*1*)). However, although it is recognized that microstructural features such as mixtures of phases and compositional variations in the host electrode material influence battery characteristics, e.g., open cell voltage, transport phenomena, and probably affect long-term stability, the mechanisms of intercalation and structural change are not well understood.

In this paper transmission electron microscopy is used to investigate the mechanism of lithium and sodium intercalation in TiS_2. Specimens of Li_xTiS_2 ($x \sim 0.5$) were prepared chemically using *n*-butyllithium and samples of Na_xTiS_2 ($0 \leq x \leq 0.6$) were prepared in Na/NaI in propylene carbonate/TiS_2 battery cells. It is shown that intercalation in both lithium and sodium cases led to a highly dislocated TiS_2 host structure. In the sodium case, there was also an inhomogeneous and complex mixture of phases typically formed. The mechanisms of intercalation and structural change are discussed and a model for the effect of microstructural inhomogeneities on the behavior of TiS_2 during cycling is considered.

Structures of TiS_2, Li_xTiS_2, Na_xTiS_2

TiS_2 is trigonal, symmetry $P\bar{3}m1$, with $a = 3.408$ Å and $c = 5.691$ Å. The structure is

* Present address: H. H. Wills Physics Laboratory, University of Bristol, Tyndall Avenue, Bristol BS8 1TL, U.K.

0022-4596/83 $3.00

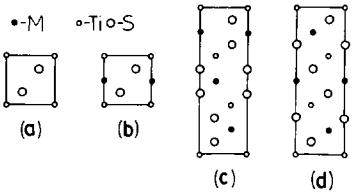

FIG. 1. Known structures for TiS_2, M_xTiS_2 (M = Li, Na) projected on to the $(11\bar{2}0)$ plane (see text).

composed of close-packed layers of sulphur or titanium atoms stacked along the c axis in the sequence AbCAbC using standard notation where capital and small letters represent sulphur and titanium layers, respectively. A projection of the structure on the $(11\bar{2}0)$ plane is illustrated in Fig. 1a.

Intercalation of Li and Na may take place in the planes between the S–Ti–S blocks. Intercalation may be accompanied by a variety of structural changes including relative sliding of the S–Ti–S blocks of the host lattice, intercalation of only a fraction of the available van der Waals layers (staging), and ordering of the alkali ion sublattice. In Li_xTiS_2 (Fig. 1b) lithium ions fill sites of trigonal antiprismatic (TAP) symmetry over the composition range $0 \leq x \leq 1$ giving a stacking sequence *Abc*[*b*]*Abc*[*b*] where the [] refers to the intercalated species. Li intercalation thus leaves the TiS_2 host structure unchanged except for changes in lattice parameter, notably an expansion of up to ~10% in the **c** direction; lattice parameters for $LiTiS_2$ are a = 3.455 Å, c = 6.195 Å (*2*). Some tendency of the lithium sublattice to order at particular compositions was reported in 1978 by Thompson (*3*). More recent work (*4–6*) has considered this as evidence of staging.

In the case of Na_xTiS_2 a variety of different phases has been identified. Rouxel and co-workers (*7*) reported a stage 2 compound (i.e., Na^+ ions occupying alternate layers) for $0.17 < x < 0.33$. A stage 1 compound was observed for $0.38 < x < 0.72$ with Na^+ ions filling sites of trigonal prismatic (TP) symmetry created by relative sliding of the S–Ti–S blocks. The stacking sequence for the TP phase is AbC[a] CaB[c]BcA[b] (Fig. 1c). For $0.79 \leq x \leq 1$ a TAP phase was identified with stacking AbC[a]BcA[b]CaB[c] (Fig. 1d). Two-phase regions were found for $0.33 < x < 0.38$ and $0.72 < x < 0.79$. Hibma (*4*) has recently reported the same phases but with different phase limits, in particular a two-phase region for the stage 2 and TP phases in the range $0.25 \leq x \leq 0.5$. In addition a stage 3 phase was observed for $x \leq 0.15$. The reasons for the discrepancies here between the work of different authors have been discussed recently (*8*). The lattice expansion along **c** is appreciably greater for intercalation of sodium compared with lithium, with lattice parameters for $NaTiS_2$ given as a = 3.469 Å, $c = 3 \times 6.86$ Å (*7*).

Experimental Procedure

Studies were carried out using nominally stoichiometric TiS_2 (Exxon Corp.) with a grain size of up to ~10 μm. Lithium-intercalated samples, Li_xTiS_2 ($x \sim 0.5$), were prepared by direct reaction with *n*-butyllithium in dry hexane. The mixture was allowed to equilibrate overnight at room temperature before the solid was filtered out, washed in dry hexane and dried under vacuum. Sodium was intercalated in battery cells with a pressed sodium anode, an electrolyte comprising glass fiber filter paper soaked in a saturated solution of NaI in propylene carbonate and a cathode of TiS_2 powder pressed at 1500 lb/in.^{2} on to a steel gauze. The three components were pressed lightly together to form an electrical contact as shown in Fig. 2. Battery assembly and subsequent cycling was carried out under dry conditions and at room temperature. Cells were cycled to give Na_xTiS_2 over the composition range $0 \leq x \leq 0.6$, the cycling being carried out by an incremental voltage stepping method (*9*) using a microprocessor

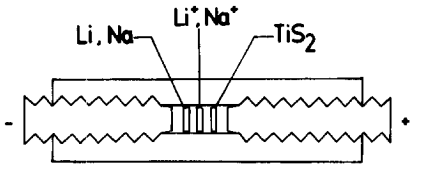

FIG. 2. Schematic illustration of Na/NaI in propylene carbonate/TiS_2 battery cells. The cell casing was PTFE with electrical contact maintained by screw-threaded stainless steel plugs.

control system. Cycling was at a rate typically ≤1 cycle/day. Cells were left to equilibrate for ½–1 day or longer before Na_xTiS_2 samples were removed, washed in dry propylene carbonate, and stored under dry conditions.

Specimens were prepared for electron microscopy by crushing as-supplied and intercalated TiS_2 powders in a mortar and pestle and dispersing the products in ethanol onto holey carbon films. Specimens were examined at 200 kV in a JEOL 200CX electron microscope operating with a $C_s \sim$ 1.2 mm and a point-to-point resolution of about 2.4 Å. Observations were also carried out at 100 kV in a JEOL 100B electron microscope. Care was taken to ensure that in

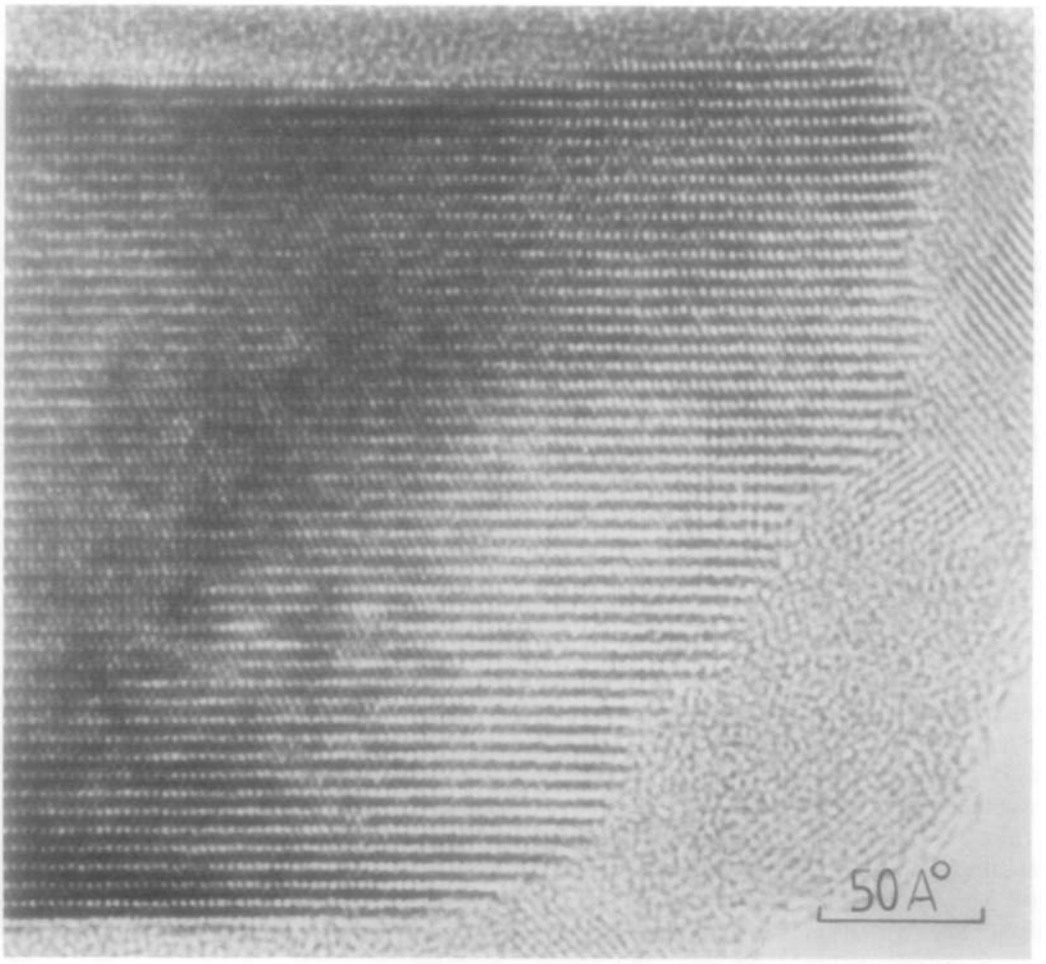

FIG. 3. $(11\bar{2}0)$ lattice image of TiS_2.

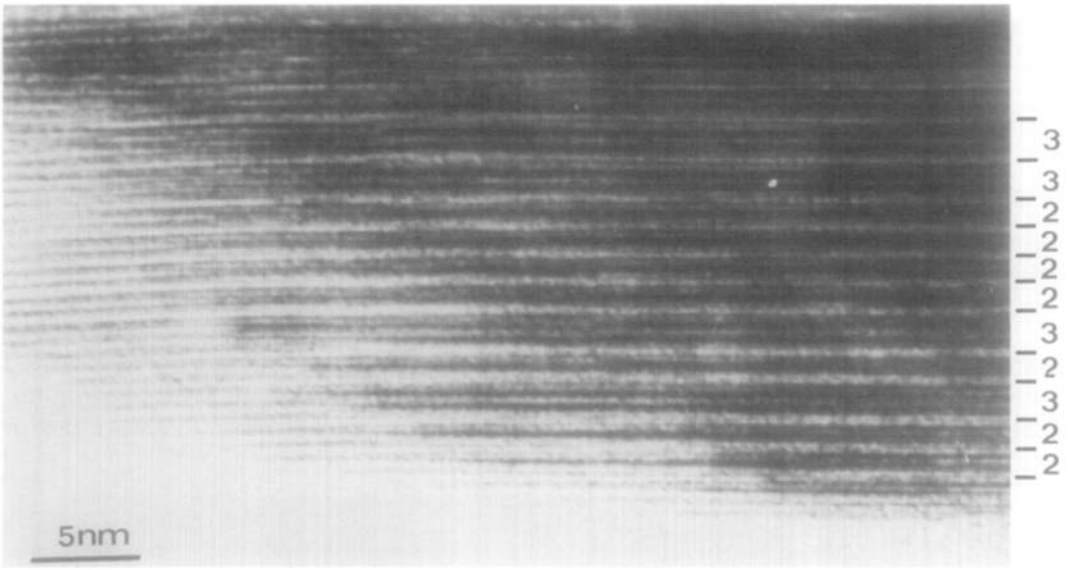

FIG. 4. Lattice image of $Na_{0.2}TiS_2$ with (0001) planes edge-on showing 2- and 3-layer staging as indicated.

the final stages of specimen preparation performed outside the dry box, and upon subsequent loading of specimens into the electron microscope, exposure to the atmosphere was kept to a minimum.

Electron Microscope Observations

Specimens of as-supplied and intercalated TiS_2 showed a high proportion, ~90–95%, of crystal platelets with normal [0001] nearly parallel to the electron beam. A few crystals, ≤5% of the total, were found to be cleaved in a plane perpendicular to (0001) such that [0001] was nearly perpendicular to the beam. Lattice imaging experiments using the JEOL 200CX electron microscope were performed on this latter type of crystal.

Figure 3 shows a $(11\bar{2}0)$ lattice image of as-supplied TiS_2. The conduction planes are viewed edge-on and run from left to right. The resolution is insufficient to give a direct correspondence between the image and the projected unit cell structure (Fig. 1a). However, the rectangular projection of the unit cell is a clear feature of the image. Observations on intercalated crystals showed wide structural variations both grain to grain and within individual grains. Figure 4 shows a crystal of Na_xTiS_2 having, nominally, $x \sim 0.2$. The lattice image, especially in the thicker regions of the crystal, shows evidence of staging with an image repeat every two or three layers in an irregular sequence as indicated. The image interpretation, especially for the thicker regions, is again not straightforward. However, taking the stated magnification (estimated accuracy ~5%) fringe spacings are approximately 3×6.18 Å and 2×6.38 Å for the 3-layer and 2-layer regions, respectively. This compares well with the results of Hibma (*4*) who gives average layer spacings for the stage 3 and stage 2 phases of 6.14 and 6.34 Å, respectively.

Figure 5 shows a crystal of nominal composition $Na_{0.5}TiS_2$. In this case the $(11\bar{2}0)$ lattice image shows evidence of three dif-

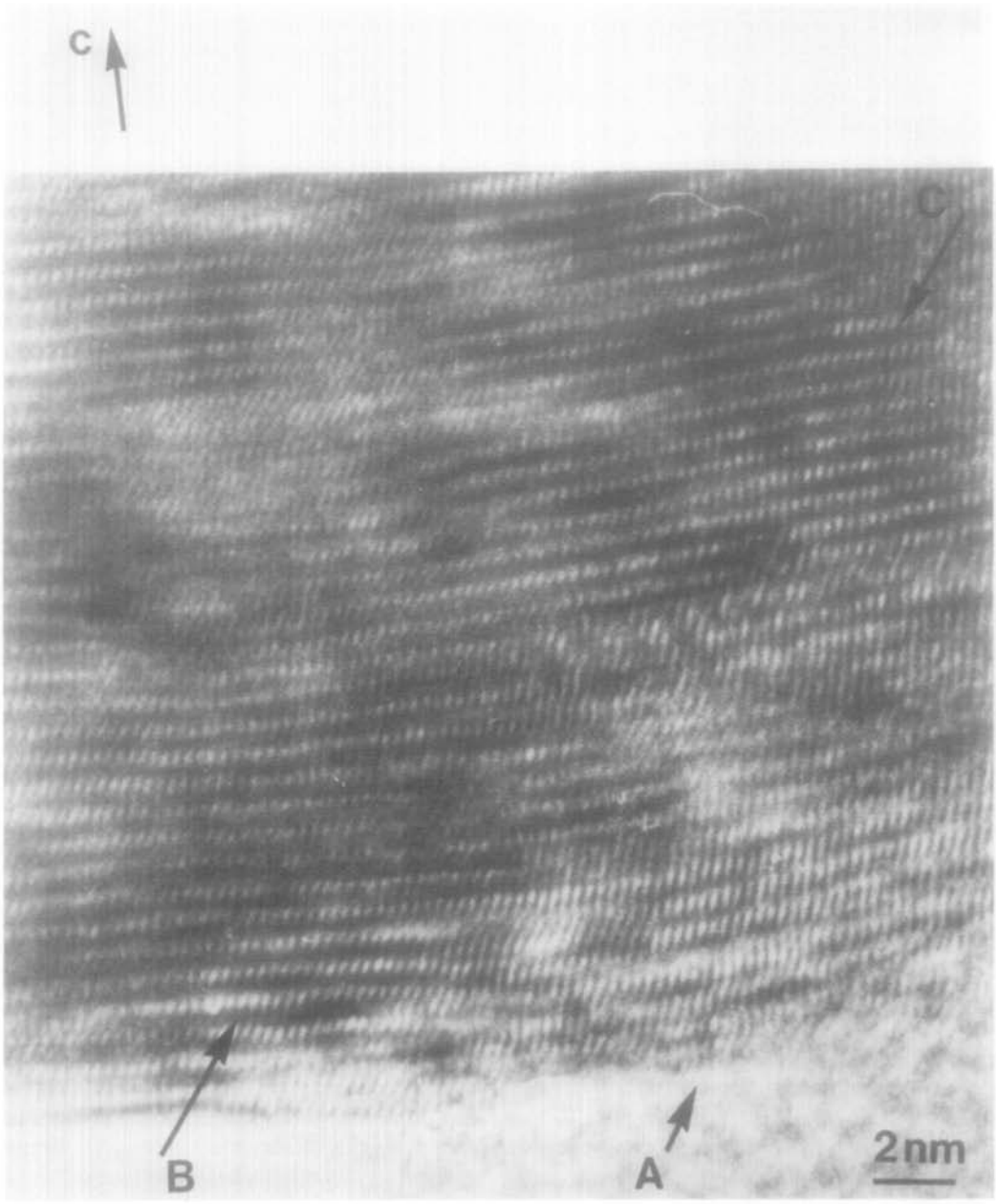

FIG. 5. $(11\bar{2}0)$ lattice image of $Na_{0.5}TiS_2$ showing different phases present (see text).

ferent phases. At A a small part of the crystal shows a rectangular spot pattern as in Fig. 3. However, in regions B and C the spot pattern is skew. The lattice image in region B is consistent with a rectangular unit cell having a 3-layer repeat along **c** and may be one of the phases in Figs. 1c or d. From the sense in which the spots are elon-

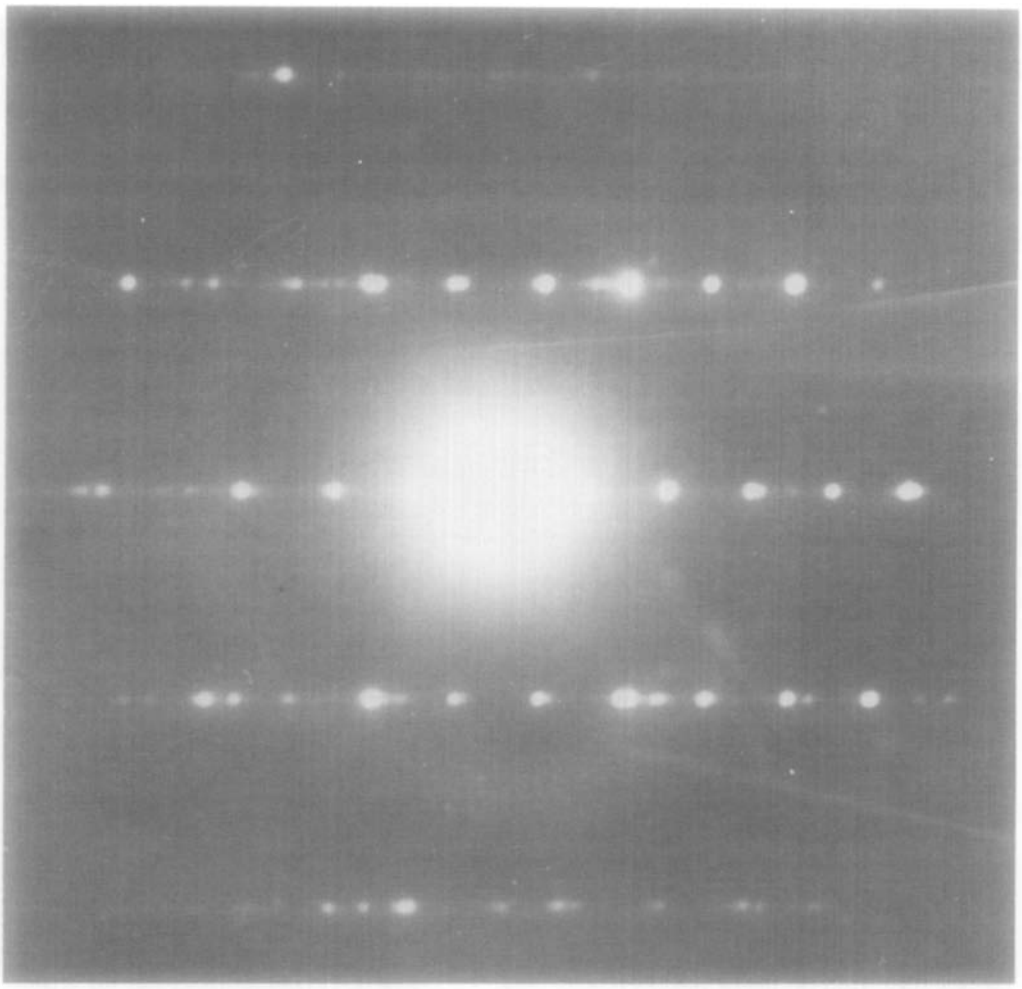

FIG. 6. Selected area diffraction pattern suggesting a 2H phase in an $Na_{0.5}TiS_2$ sample ((110) section).

gated and by comparison with images computed using a multislice approach (*10*) the image was found to be consistent with the TP phase in Fig. 1c. Taking the repeat distance perpendicular to **c** as 2.96 Å (corresponding to $a = 3.43$ Å), the **c** spacing is 6.9 Å in reasonable agreement with known values for the TP phase (6.98 Å, $x = 0.55$ (*7*)). The image at C suggests a unit cell with a 2-layer repeat. Confirmation that this represents a distinct phase is given by the selected area diffraction pattern in Fig. 6. The structure of this phase is uncertain; the shearing of S–Ti–S blocks by a half unit appears unlikely as the site coordination in the conduction plane becomes asymmetrical. A model where the stacking is altered in the S–Ti–S blocks may produce a 2-layer repeat. Such a transformation occurs in the 1T to 2H transition which some metal dichalcogenides exhibit (*1*). Recent work on sodium intercalation in $Na_xN_x^{3+}M_{1-x}S_2$ compounds (M = Zr, Sn, N = Y, In, etc.) (*11–13*) has shown the existence of a 2H phase at compositions x intermediate to those producing TP and TAP phases of the

types in Figs. 1c and d. The stacking sequence in the 2H phase can be AbC[a] CbA[b] or AbC[b]CbA[c] depending on the ionicity of the host structure. There is evidence for a 2H phase in chemically prepared Na_xTiS_2, but only at elevated temperatures (*14*). Further experiments are required to elucidate the detailed cell structure here.

Figure 7 shows another crystal of nominal composition $Na_{0.5}TiS_2$. This crystal shows a region A exhibiting staging with 2- and 3-layer repeats. B shows an area with the TP phase. The average **c** spacings in regions A and B are approximately 6.3 and 7.0 Å, respectively, representing a misfit close to 10%. The mismatch is partly accommodated by a terminating conduction plane at C representing a dislocation having a component of Burgers vector along **c**. The bending of the crystal and the original transformation from the TAP phase may both be described by dislocations with Burgers vectors having components perpendicular to **c**. The situation is illustrated schematically in Fig. 7. Within a single

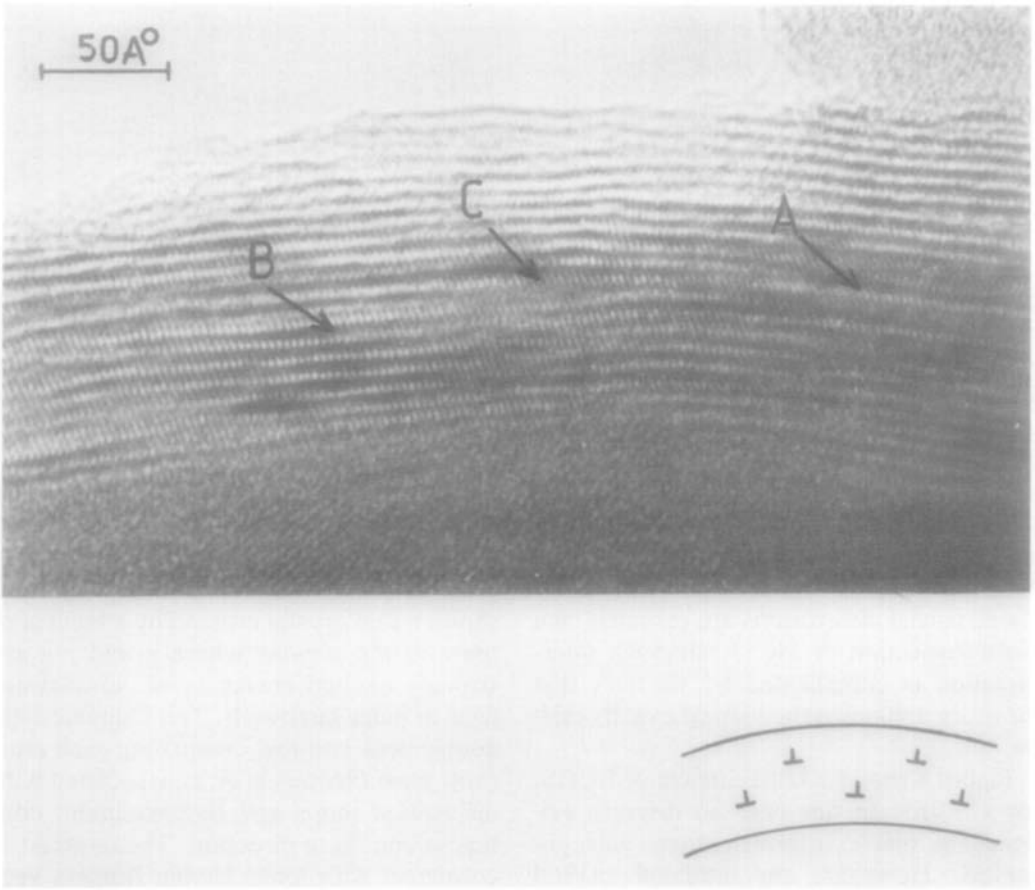

FIG. 7. $(11\bar{2}0)$ lattice image of $Na_{0.5}TiS_2$. In addition to the different phases present, e.g., at *A* and *B*, there are dislocations accommodating mismatch strains, e.g., at *C*, as well as other dislocations describing the bending of the crystal and possibly also phase transformations as illustrated schematically.

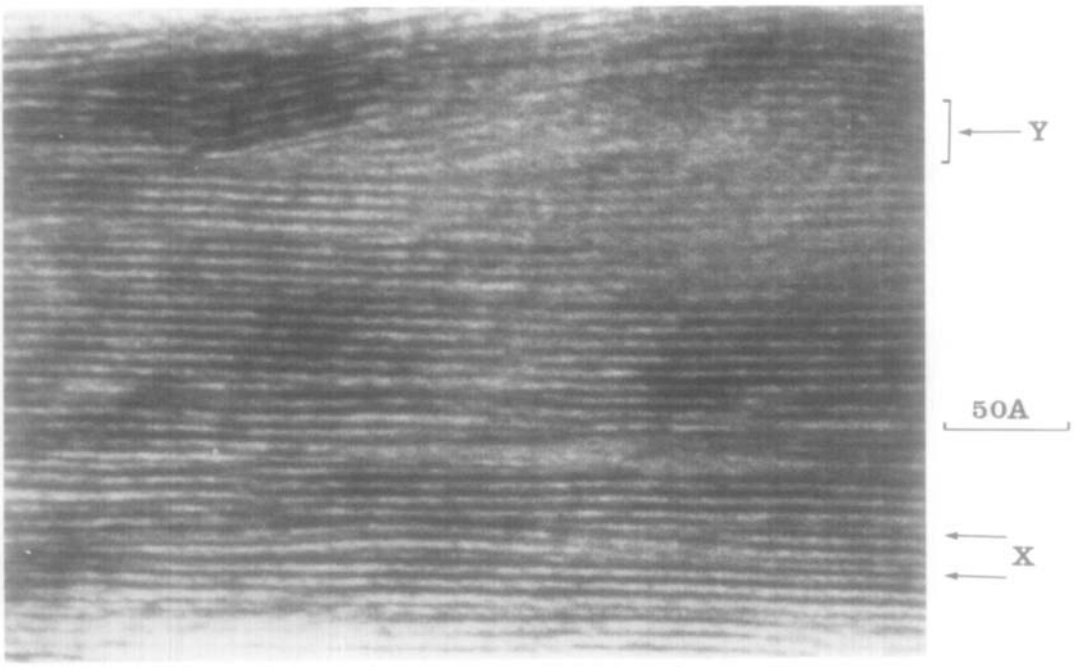

FIG. 8. Lattice image of Li_xTiS_2 ($x \sim 0.5$) with conduction planes running left to right.

phase dislocations must have a total Burgers vector given by a lattice translation vector, e.g., $\mathbf{b} = \frac{1}{3}\langle 11\bar{2}0\rangle$ for basal plane dislocations. On the other hand, phase transformations in Na_xTiS_2 involve a change in stacking sequence (see earlier) and may be described by partial dislocations of $\frac{1}{3}\langle 10\bar{1}0\rangle$ type. Diffraction contrast studies show that both types are present in Na_xTiS_2 samples. Some examples of inclined partial dislocations are revealed by a close inspection of Fig. 7, although interpretation is complicated by the fact that these are unlikely to be viewed exactly end-on.

Figure 8 shows a lattice image of Li_xTiS_2 for $x \sim 0.5$. In this case no discrete evidence of phase transformations was observed. However, the lithiated crystal shows a high density of faults in the layer stacking. One type of fault is seen at *X*. As indicated by the arrows there is a platelet of extra material viewed edge-on and an adjacent plane where a segment of material is missing. The two defects constitute dislocation loops whose components of Burgers vectors along **c** are opposite. *Y* shows a gross fault in the layer stacking with an inclusion of material up to ~40 Å thick.

The types of fault in Fig. 8 are readily apparent in diffraction contrast. Figures 9 and 10 show $Li_{0.5}TiS_2$ crystals viewed approximately along the *c* axis. Figure 9 shows a thin crystal crossed by a bend contour. In the regions where **g** and $-\mathbf{g}$ are strongly excited crescents of contrast appear in pairs (arrowed). The characteristic double peak contrast comprising each crescent, most obvious at A, is associated with dislocation loops and has maximum contrast along the **g** direction. The contrast is consistent with loops having Burgers vector **b** along the diffraction plane normal, i.e., along **c**. In this case $\mathbf{g} \cdot \mathbf{b} = 0$ but displacements of the diffracting planes still occur with magnitude proportioned to

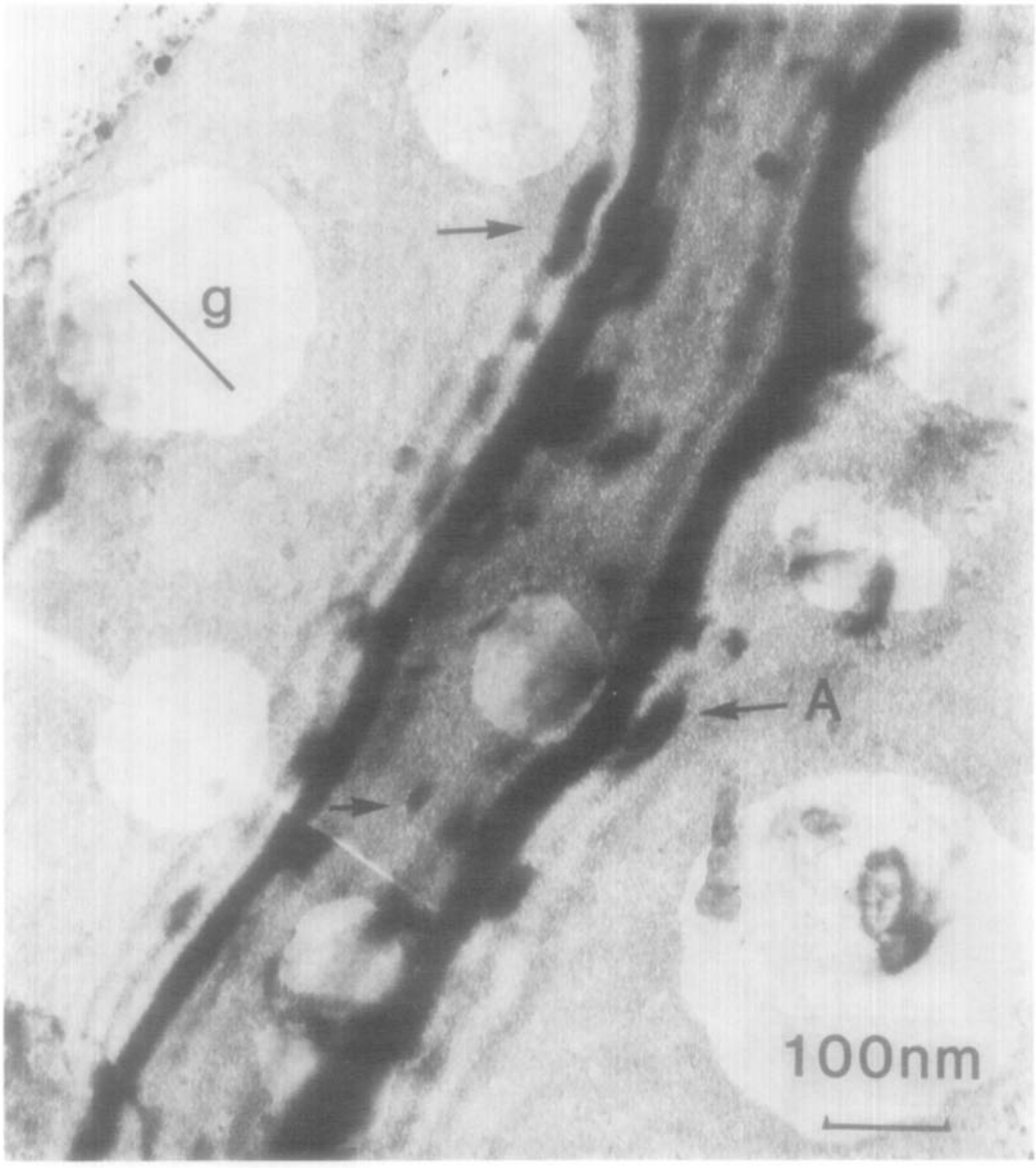

FIG. 9. Bright field micrograph of a Li_xTiS_2 ($x \sim 0.5$) crystal viewed approximately down the c axis. Loops with $\mathbf{g} \cdot \mathbf{b} = 0$ (i.e., **b** parallel to **c**) are visible in residual contrast close to the bend contour. The crystal is thin enough such that the holes in the carbon support film are clearly visible.

$\mathbf{g} \cdot (\mathbf{b} \times \mathbf{u})$ where **u** is the dislocation line direction. The contrast is thus expected to be a maximum for **u** perpendicular to **g** as observed. The double peak contrast is characteristic of this type of image (*15*). The dark field image in Fig. 10 shows a high density of dislocation loops ~50–100 Å across. The contrast of features similar to *X* may be understood as due to gross inclusions as in Fig. 8 (*Y*). A tentative explanation for the contrast along these lines is illustrated in Fig. 11. This depicts a situation

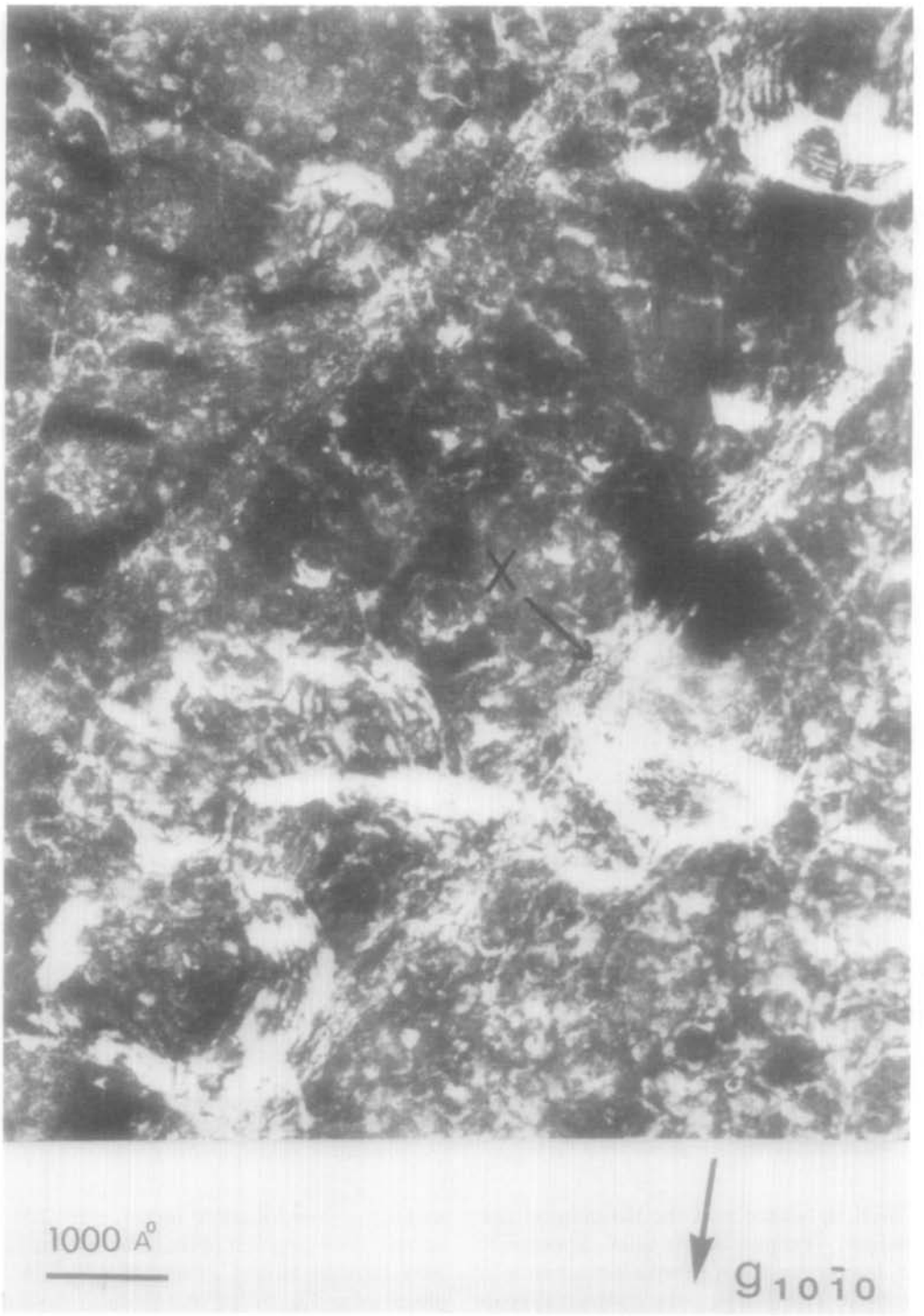

FIG. 10. Dark field micrograph in $\mathbf{g} = 10\bar{1}0$ of an Li_xTiS_2 ($x \sim 0.5$) crystal.

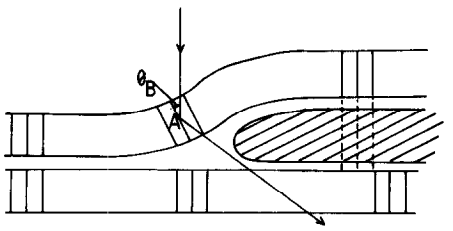

FIG. 11. Tentative explanation for the contrast of feature *X* in Fig. 10 (see text).

where a layer section of the TiS_2 crystal has formed a blister on the crystal surface due to a relatively large inclusion such that equivalent lattice planes in the upper and lower halves of the TiS_2 become displaced (illustrated schematically). Under these conditions displacement fringes are formed, although the spacing (≤40 Å experimentally) will depend on a number of factors including the nature and thickness of the inclusion and the bending as well as the relative displacement of the diffracting planes. The relatively strong diffraction from the edge of the defect *X* may be explained by local bending of the diffracting planes towards the Bragg position. However, whether defects such as *X* are a true feature of intercalation or an artefact of specimen preparation is, along with the nature of the inclusions, uncertain at present.

Diffraction contrast experiments on Na-intercalated samples also showed highly dislocated crystals. The dislocation structure was considerably more complex than observed in Li_xTiS_2 due to the presence of different phases. Experiments are continuing to analyze the dislocation structure in these samples.

Discussion

The observations on Na_xTiS_2 show that sodium intercalation is complex in our experiments leading to a wide range of phases distributed inhomogeneously on a fine scale. The observations show variable staging at low levels of sodium intercalation ($x \sim 0.2$) and a mixture of phases requiring transformations of the host lattice at higher levels of intercalation ($x \sim 0.5$). The results indicate a phase not previously reported for Na_xTiS_2 (Figs. 5, 6).

It is worth considering the effects of an inhomogeneous distribution of phases and of **c** spacings on the host TiS_2 crystal. As seen in Fig. 7 the effect of variable **c** spacings is that the TiS_2 host structure requires dislocations with Burgers vectors having components along **c**. Taking the component of Burgers vector along **c** as $b_c = |\mathbf{c}|$ variations in **c** of up to 10% require a dislocation spacing of $10|\mathbf{c}|$ or 60 Å. Phase transformations requiring relative shearing of the layers may be described by dislocations with Burgers vectors perpendicular to **c**. Whether these phase transformations proceed by movement of such transformation dislocations has not yet been determined. However, recent experiments have demonstrated that phase transformations can occur under the action of the electron beam. Figure 12 shows an example where a TAP–TP phase transformation has taken place. The mechanism is as yet uncertain but may involve changes in chemical composition as observed in other fast ion conductors, for example in β-alumina (*16*). Analysis of images such as Fig. 12 suggests that discrete transformation dislocations as in Fig. 7 do indeed migrate in phase transformations.

The result of the inhomogeneities in the structure of Na_xTiS_2 crystals is, therefore, to generate a high dislocation density. As dislocations move and interact we may suppose that the introduction of dislocations is not entirely reversible during cycling. This is, of course, well known in phenomena such as fatigue. The dislocation density may thus tend to increase as the number of cycles increases.

The observations of high densities of dislocations in the chemical intercalation of Li_xTiS_2 is particularly interesting. Although

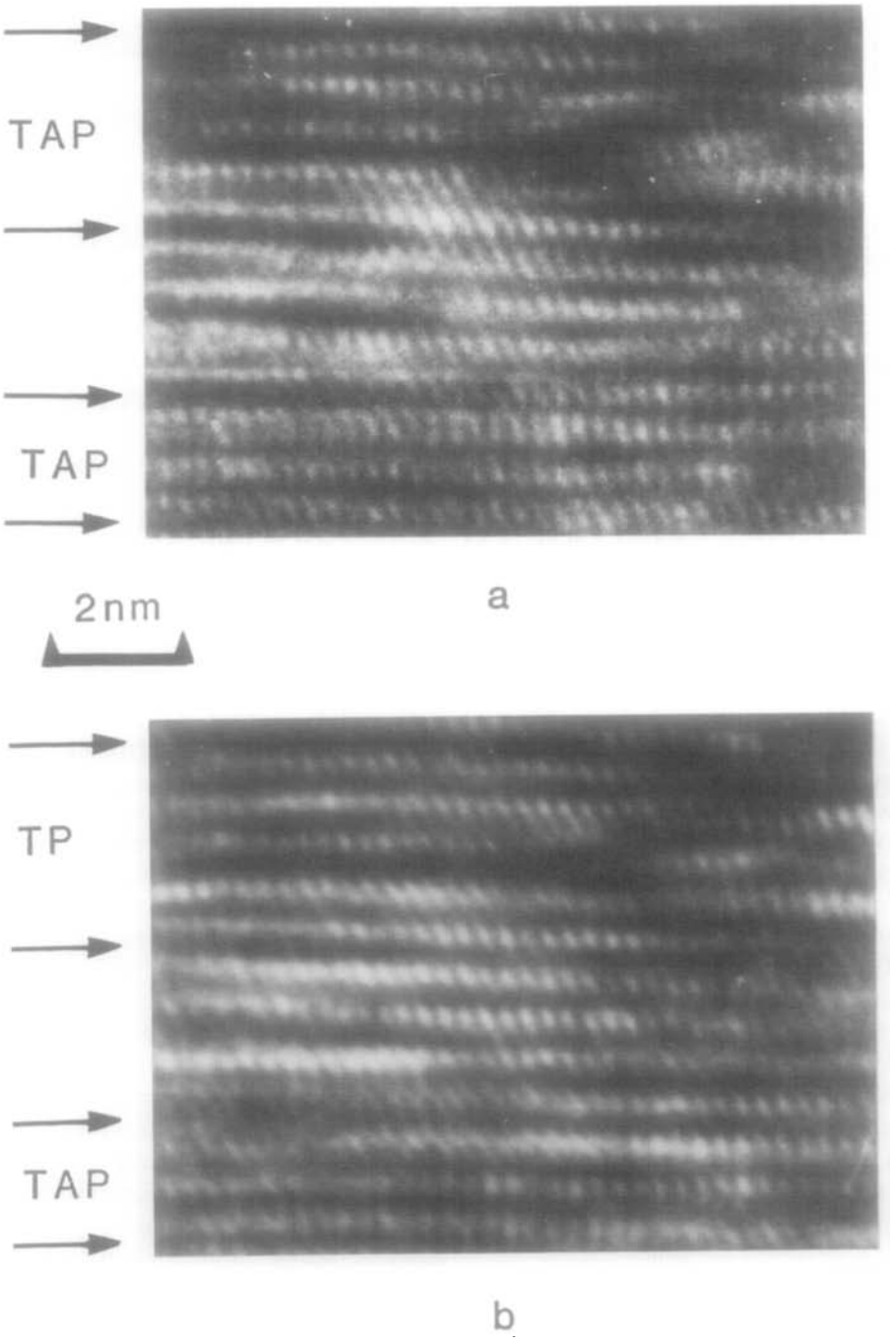

FIG. 12. ($11\bar{2}0$) lattice images of the same area of a Na_xTiS_2 ($x \sim 0.5$) crystal photographed in sequence (top = earlier image) showing a phase transformation under the action of a focused 200-kV electron beam (JEOL 200CX microscope).

no structural changes occur in the TiS_2 host lattice the results imply (1) that strains arise due to the formation of stable domains of differing lithium content, or (2) that the high rates of chemical intercalation result in nonequilibrium concentration gradients. Experiments to investigate domain formation and to examine the signification of intercalation rate by carrying out more controlled synthesis using Li/TiS_2 batteries are in progress.

Acknowledgments

We are grateful to Dr. P. J. Wiseman of the Inorganic Chemistry Laboratory, Oxford University, for help in preparing the lithiated TiS_2 samples, to Professor J. Rouxel for a copy of a forthcoming paper (Ref. *8*), and to the CEGB for financial support.

References

1. M. S. WHITTINGHAM, *Prog. Solid State Chem.* **12,** 1 (1978).
2. M. S. WHITTINGHAM, *J. Electrochem. Soc.* **123,** 315 (1976).
3. A. H. THOMPSON, *Phys. Rev. Lett.* **40-23,** 1511 (1978).
4. T. HIBMA, *J. Solid State Chem.* **34,** 97 (1980).
5. J. R. DAHN AND R. R. HAERING, *Solid State Commun.* **40,** 245 (1981).
6. J. R. DAHN, D. C. DAHN, AND R. R. HAERING, *Solid State Commun.* **42,** 179 (1982).
7. J. ROUXEL, M. DANOT, AND J. BICHON, *Bull. Soc. Chim. Fr.* 3930 (1971); J. Bichon, M. Danot, and J. Rouxel, *C.R. Acad. Sci.* **276,** 1283 (1973); A. Leblanc-Soreau, M. Danot, L. Trichet, and J. Rouxel, *Mater. Res. Bull.* **9,** 191 (1974).
8. P. MOLINIE, L. TRICHET, J. ROUXEL, C. BERTHIER, Y. CHABRE, AND P. SEGRANSAN, *J. Phys. Chem. Solids,* to be published.
9. A. H. THOMPSON, *J. Electrochem. Soc.* **126,** 608 (1979).
10. A. J. SKARNULIS, D. L. WILD, G. R. ANSTIS, C. J. HUMPHREYS, AND J. C. H. SPENCE, *Inst. Phys. Conf. Ser.* **61,** 347 (1981).
11. L. TRICHET AND J. ROUXEL, *Mater. Res. Bull.* **12,** 345 (1977).
12. P. COLOMBET, M. DANOT, AND J. ROUXEL, *Mater. Res. Bull.* **14,** 813 (1979).
13. J. ROUXEL, "Fast Ion Transport in Solids" (P. Vashishta *et al.*, Eds.), p. 125, Elsevier–North-Holland, 1979.
14. R. J. HAANGE, A. J. A. BOS-ALBERINK, AND G. A. WIEGERS, *Ann. Chim. (Paris) Sci. Mater.* **3,** 201 (1978).
15. A. HOWIE AND M. J. WHELAN, *Proc. R. Soc. A* **267,** 206 (1962).
16. R. HULL, D. CHERNS, C. J. HUMPHREYS, AND J. L. HUTCHISON, *Inst. Phys. Conf. Ser.* **61,** 23 (1981).